Chapter 3

THE $\tilde{A} \leftarrow \tilde{X}$ TRANSTION OF THE NITRATE RADICAL (NO_3): ELUCIDATION OF THE NON-ADIABATIC EFFECTS

3.1 Introduction to the chemical physics problem of NO_3

The nitrate radical NO_3 is an important nighttime oxidant, playing key roles in both gas phase and aerosol chemistry.[1-3] As we focus on the atmospheric role of NO_3 in Chapter 4, we discuss here the chemical physics problem of NO_3. Spectra of NO_3 were observed in the visible region as early as 1882.[4] In 1953, Walsh analyzed the molecular bonding orbitals of NO_3 and found that the radical favored a planar D_{3h} configuration in the ground state: $...(4e')^4(1e'')^4(1a_2')^1$ (Fig. 3.1).[5] With only four atoms and apparent D_{3h} symmetry, NO_3 appeared to be a simple system to study. After a century of extensive theoretical and experimental effort, the "simple" open-shell radical NO_3 however continues to provoke more questions than answers today.

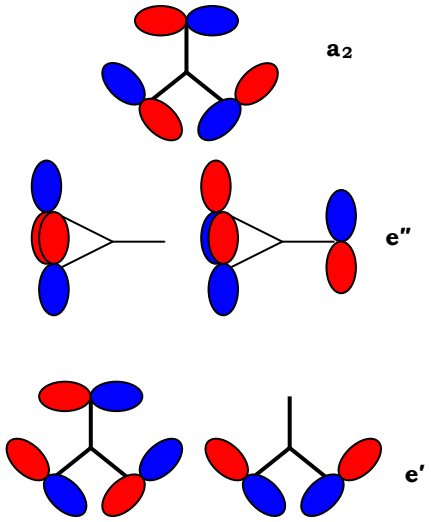

Figure 3.1. Diagram of the molecular bonding orbitals of NO_3

The non-adiabatic effects of NO_3, specifically the Jahn Teller (JT) and pseudo-JT (PJT) effects, complicate study of the radical. The Born-Oppenheimer (BO) approximation, or the separation of nuclear and electronic motions, is commonly invoked to simplify solutions to the Schrödinger equation. The JT effect is a classic example of the breakdown of the BO approximation. The theorem states that a molecule in a degenerate electronic orbital state distorts to a lower symmetry to remove the degeneracy.[6] The PJT effect extends the theorem to molecules whose electronic states are nearly degenerate.[7,8] Both JT and PJT effects have been reviewed in the literature.[9,10] We also provide a more detailed description in Appendix 3.1

Most dynamic studies probe the asymptotic behaviors of reactions to learn about the non-adiabatic effects. In the JT studies, the bound molecules are spectroscopically probed such that the distortion can be observed directly. Various chemical systems have been shown to undergo JT distortion, including the cyclopentadienyl radical C_5H_5, the benzene cation $C_6H_6^+$, the silver trimer Ag_3, and the methoxy radical CH_3O.[9] NO_3 provides a unique opportunity to study both JT and PJT effects in the same chemical system.

The three lowest electronic states of NO_3 are the $\tilde{X}^2A_2'$, $\tilde{A}^2E''$, and $\tilde{B}^2E'$ states. Spaced approximately an eV apart, the two upper electronic states are JT active, and all three are pseudo-JT coupled (Fig. 3.2). The extent of the strength of these vibronic interactions in NO_3 has been heavily debated.[11-14] Of the three electronic states, the ground state $\tilde{X}^2A_2'$ has been the most studied (Table 3.1).[12,13,15-24] Most groups have agreed on assignment of D_{3h} symmetry to the ground state.

Study of the $\tilde{A}^2E''$ and $\tilde{B}^2E'$ excited states has been more challenging. Both states are JT active. While the symmetric stretch and out-of-plane (oop) umbrella modes, $\upsilon_1''(a_1')$ and $\upsilon_2''(a_1'')$, are non-degenerate, the antisymmetric stretch and antisymmetric in-plane bending modes, $\upsilon_3''(e')$ and $\upsilon_4''(e')$, are degenerate. Study of the JT effect in the excited states therefore becomes a bimodal JT problem. To further complicate matters, the $\tilde{A} \leftarrow \tilde{X}$ transition is electric-dipole forbidden. Therefore, studies of the excited states of NO_3 have historically been restricted to studies of the $\tilde{B}$ state.

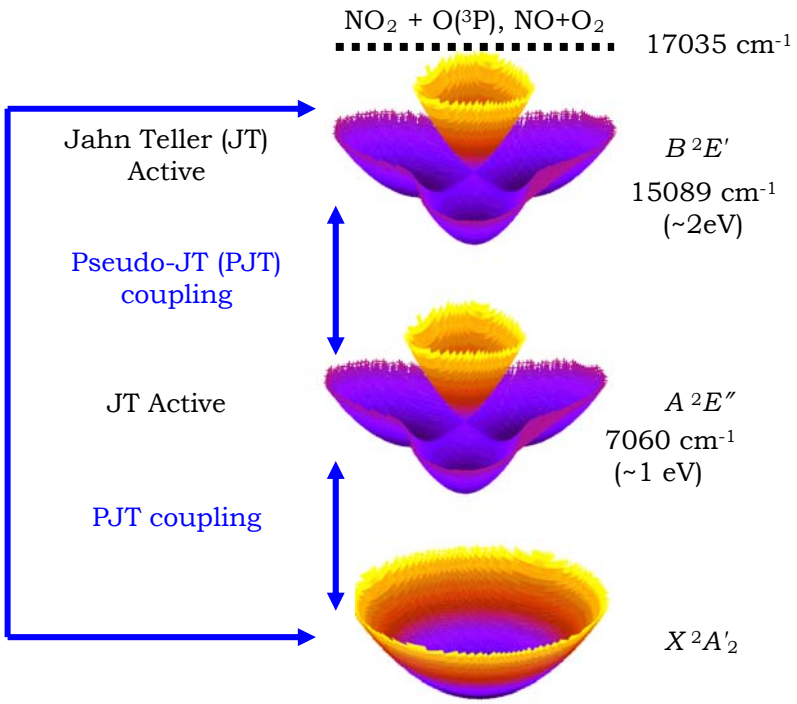

Figure 3.2. Schematic of the three lowest electronic states of NO_3

Jones and Wulf first assigned the $\tilde{B} \leftarrow \tilde{X}$ transition of NO_3 in 1937.[25] The transition is very strong, with $\sigma_{662\ nm} = 2.2 \times 10^{-17}$ cm^2.[18-20] Atmospheric groups have used these bands to quantify NO_3 concentrations at ambient conditions in the troposphere.[26-30] The $\tilde{B} \leftarrow \tilde{X}$ bands however are not ideal for spectroscopic studies, as the bands are greatly broadened by strong vibronic interactions. Efforts to resolve the bands using jet cooling have proven difficult.[31] Structural details of the $\tilde{B}$ state are not readily available.

In this work, we turn to the dark $\tilde{A}$ state of NO_3 to shed light on the non-adiabatic effects of NO_3. While the $\tilde{A} \leftarrow \tilde{X}$ transition is dipole forbidden, there are still ways to study the dark excited $\tilde{A}$ state. In the next section, we discuss the relatively brief experimental and theoretical history of the $\tilde{A}$ state and outline our specific goals for studying the $\tilde{A}$ state of NO_3.

Recent theoretical studies of the ground state frequencies

	Frequency	Method	Reference
$\upsilon_1''(a_1')$	1051.2	LVC	Stanton, JCP 2007
	1150	EOMIP-CCSD//DZP	Crawford & Stanton, JCP 2000
	1140.6	MR-SDCI//DZP	Eisfeld & Morokuma JCP 2000
	1083.5	MR-SDCI + Davidson/AVTZ-f	Eisfeld & Morokuma JCP 2001
	1133	EOMIP-CCSD//TZ2P	Wladyslawski & Nooijen 2002
$\upsilon_2''(a_2'')$	796	EOMIP-CCSD//DZP	Crawford & Stanton, JCP 2000
	756.8	MR-SDCI//DZP	Eisfeld & Morokuma JCP 2000
	773.0	MR-SDCI + Davidson//AVTZ-f	Eisfeld & Morokuma JCP 2001
	814	EOMIP-CCSD//TZ2P	Wladyslawski & Nooijen 2002
$\upsilon_3''(e')$	994.3	LVC	Stanton, JCP 2007
	1146	EOMIP-CCSD//DZP	Crawford & Stanton, JCP 2000
	1439.2	MR-SDCI//DZP	Eisfeld & Morokuma JCP 2000
	1376.5	MR-SDCI + Davidson//AVTZ-f	Eisfeld & Morokuma JCP 2001
	1113	EOMIP-CCSD//TZ2P	Wladyslawski & Nooijen 2002
$\upsilon_4''(e')$	361	LVC	Stanton, JCP 2007
	246	EOMIP-CCSD//DZP	Crawford & Stanton, JCP 2000
	173.5	MR-SDCI//DZP	Eisfeld & Morokuma JCP 2000
	272.9	MR-SDCI + Davidson//AVTZ-f	Eisfeld & Morokuma JCP 2001
	249	EOMIP-CCSD//TZ2P	Wladyslawski & Nooijen 2002

Previous experimental studies of the ground state frequencies

	Frequency	Method	Reference
$\upsilon_1''(a_1')$	1060	LIF	Ishiwata JPC 1983
	1050/931	LIF	Nelson JPC 1983**
	1053	LIF	Kim JCP 1992
$\upsilon_2''(a_2'')$	753	LIF	Kim JCP 1992
	762	FTIR	Friedl & Sander JPC 1987
	763.1	Ne matrix	Jacox & Thompson JCP 2008
$\upsilon_3''(e')$	1480	LIF	Ishiwata JPC 1983
	1489/1166	LIF	Nelson JPC 1983**
	1500	LIF	Kim JCP 1992
	1492.393	IR diode	Kawaguchi JCP 1990 (analysis)
	1000-1100	Ne matrix	Jacox & Thompson JCP 2008
$\upsilon_4''(e')$	365	CRDS	Deev JCP 2005*
	380	LIF	Ishiwata JPC 1983
	360/418	LIF	Nelson JPC 1983**
	368	LIF	Kim JCP 1992
	365.6	Ne matrix	Jacox & Thompson JCP 2008
	365.48419	FTIR	Kawaguchi, J. Mol. Spec. 2011 (submit)

*used origin 7064 cm^{-1}

**assumed ground state in C_{2v} symmetry

Table 3.1. The upper table lists the most recent theoretical values of the ground state frequencies of NO_3. The lower table lists experimental values. Most groups have agreed that the ground state has D_{3h} symmetry. The most significant experimental disparity is in the value of the $\upsilon_3''(e')$ frequency.

3.2 The dark $\tilde{A}$ state of NO_3

The $\tilde{A}$ state of NO_3 was observed for the first time twenty years ago in a low resolution anion photoelectron spectrum (PES) of the nitrate anion NO_3^-. The origin of the $\tilde{A}$ state was estimated to be in the near-infared (NIR) region at $T_0(\tilde{A})$ = 7000(100) cm^{-1}.[32] Hirota *et al.* and Kawaguchi *et al.* recognized that the $\tilde{A}$ state could also be studied using spectroscopic absorption methods in the NIR via Herzberg-Teller selection rules (Fig. 3.3).[33,34] The HT selection rules state that a transition is allowed only if the product of the electric dipole transition moment and the initial and final vibronic states contain the totally symmetric representation of the molecular system's point group.

For NO_3, the origin of the $\tilde{A} \leftarrow \tilde{X}$ transition is electric dipole forbidden:

$$0_0^0 : a_1' \notin A_2' \otimes \{\mu_{\parallel}(a_2'') \oplus \mu_{\perp}(e')\} \otimes E'' . \tag{3.1}$$

However, vibronic bands of the $\tilde{A} \leftarrow \tilde{X}$ transition such as the parallel and perpendicular bands, 4_0^1 and 2_0^1 respectively, are HT allowed:

$$4_0^1 : a_1' \in A_2' \otimes \mu_{\parallel}(a_2'') \otimes \{E'' \otimes \upsilon_4'(e')\} = A_2' \otimes \mu_{\parallel}(a_2'') \otimes \{a_1'' \oplus \cancel{a_2''} \oplus \cancel{e''}\} \tag{3.2}$$

$$2_0^1 : a_1' \in A_2' \otimes \mu_{\perp}(e') \otimes \{E'' \otimes \upsilon_2'(a_2'')\} = A_2' \otimes \mu_{\perp}(e') \otimes \{e'\} . \tag{3.3}$$

Hirota *et al.* and Kawaguchi *et al.* collected rotationally resolved spectra of the 4_0^1 and 2_0^1 bands using diode laser and Fourier transform infrared (FTIR) spectroscopy respectively. Both the upper and lower rotational constants were assigned for the 4_0^1 band.

Our group and Jacox and Thompson followed with surveys of the $\tilde{A} \leftarrow \tilde{X}$ vibronic bands in the 5000-9000 cm^{-1} region using cavity ringdown spectroscopy (CRDS) of NO_3 in the gas phase and FTIR spectroscopy of NO_3 in the matrix, respectively.[24,35,36] Multiple vibronic bands were observed and assigned in the spectra. Appendix 3.2 provides a more detailed overview of the previous CRDS survey.

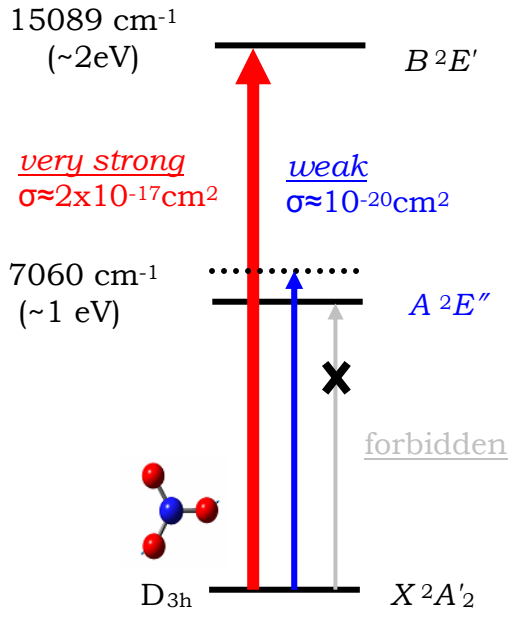

Figure 3.3. Schematics of the transitions to the excited electronic states of NO_3. While the absorption cross section for the $\tilde{B} \leftarrow \tilde{X}$ transition is quite strong, much of the structural information about NO_3 is learned from the weak $\tilde{A} \leftarrow \tilde{X}$ transition of NO_3, as spectra of the $\tilde{A} \leftarrow \tilde{X}$ transitions can be rotationally resolved.

Theoretical work on the $\tilde{A}$ state has increased only in the last decade. Multi-reference configuration interaction (MRCI) calculations by Eisfeld *et al.* predict a large JT distortion in the $\tilde{A}$ state, with C_{2v} minimum B_1 (depth 2000 cm^{-1}) and transition state A_2 (pseudorotation barrier 1000 cm^{-1}).[16] The calculated JT stabilization energies are much larger in magnitude than the spin-orbit couplings (~50-150 cm^{-1}) of similar-sized

JT systems, such as the methoxy radical.[37-39] In many NO_3 models, the spin-orbit coupling is thus ignored.

Improvements to the *ab initio* models initially involved incorporation of higher order JT terms.[16,40,41] The growing experimental evidence for strong PJT effects in NO_3 led many groups to use the linear multimode vibronic coupling (LVC) model developed by Koppel, Domcke, and Cederbaum.[42] To date, Faraji *et al.* have used the model to simulate Weaver's anion PE spectrum,[43] while Stanton has used the model to simulate band intensities of our previously published CRD spectrum.[44,45] As theoretical models of the $\tilde{A}$ state continue to evolve, we need more experimental benchmarks on the $\tilde{A}$ state of NO_3.

The vibrational frequencies of the $\tilde{A}$ state would provide a first means to test the accuracy of the theoretical models. While many $\tilde{A} \leftarrow \tilde{X}$ bands were assigned in the previous CRD and matrix studies, vibrational frequencies of the $\tilde{A}$ state were not able to be definitively determined due to the lack of an assignment of the origin band. Values were instead inferred from spacing between combination bands. Identification of the origin band would lead to absolute fundamental frequencies of the $\tilde{A}$ state of NO_3.

The origin of the $\tilde{A} \leftarrow \tilde{X}$ transition of NO_3 however has yet to be observed in the gas phase. While the transition is electric dipole forbidden, in principle, we should be able to observe the origin directly via magnetic dipole selection rules. Magnetic transitions are very weak, typically 10^{-5} the strength of electric transitions.[46] Only a handful of such studies have been done on polyatomic molecules, including oxygen and formaldehyde.[47-50] We would need a very sensitive technique to observe the origin band of NO_3.

Previous experiments have also provided only a qualitative gauge of the JT strength in the $\tilde{A}$ state. The importance of the JT effect in NO_3 was apparent in the first PES experiment when Weaver *et al.* observed a strong progression by the Franck-Condon (FC) forbidden υ_4' frequency in the $\tilde{A}$ state that could only be explained by strong vibronic coupling among the three lowest electronic states of NO_3.[32] In our previous CRD survey, we observed a series of irregularly spaced 4_0^n (n = 1-4) bands. The rotational contours of the bands were fit with symmetric top models; however, the irregular progression of the bands supported small to moderate JT activity along the Q_4 coordinate. We also observed surprisingly similar strength absorptions by the parallel 4_0^1 and perpendicular 2_0^1 bands. The intensity borrowing mechanisms for the respective bands highlighted the strong vibronic coupling among the three lowest electronic states of NO_3 (Appendix 3.2).[44]

The matrix isolation survey supported our gas phase observations. In addition to $^{14}NO_3$, Jacox and Thompson also examined isotopologues of NO_3 that reduced the symmetry of the radical to C_{2v}. They observed additional satellites and shoulders to absorption features that were attributed to matrix effects. They however did not observe any apparent splitting in the vibronic bands from reduced symmetry.

A quantitative measure of the vibronic strength in the $\tilde{A}$ state would provide a better benchmark for *ab initio* models of NO_3 and would offer valuable insight into the strength of the nonadiabatic effects of NO_3. Many of the previous studies focused on the JT activity along the Q_4 coordinate. The $\tilde{A}\,^2E'' \otimes \upsilon_4(e')$ manifold of the $\tilde{A}$ state is split into three vibronic levels: $a_1'' \oplus a_2'' \oplus e''$ (Fig. 3.4). The ordering and magnitude of the

splitting are direct consequences of the strengths of vibronic interactions in NO_3. Only the a_1'' level has been examined via the 4_0^1 band, as transitions to the a_2'' and e'' vibronic levels are forbidden from the ground state under HT selection rules. Access to the e" level is allowed via the 4_1^1 hot band, as the symmetry of the ground state is changed. Measurement of the e''-a_1'' splitting would provide the first quantitative gauge of the JT effect.

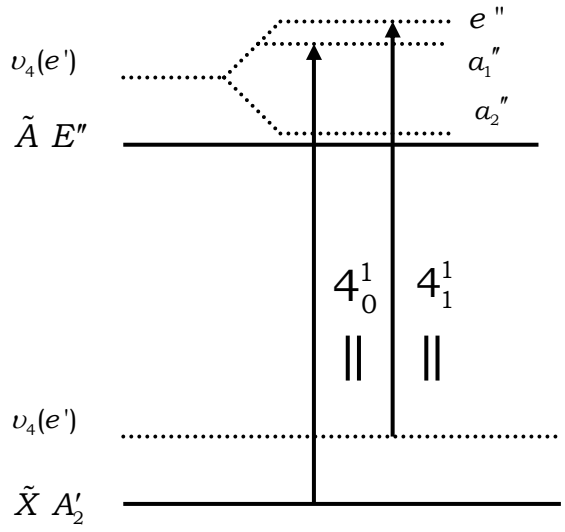

Figure 3.4. Schematic of the $\tilde{A}^2E'' \otimes \upsilon_4(e')$ manifold of the Ã state. To date, only the a_1'' level has been examined. We access the e'' level via the 4_1^1 hot band.

In this work, we use the sensitivity of the pulsed CRDS apparatus to examine the origin and hot bands of the $\tilde{A} \leftarrow \tilde{X}$ transition of NO_3 in the 7000-7650 cm^{-1} region and to measure directly the fundamental vibrational frequencies and JT strength of the $\tilde{A}$ state of NO_3.

3.3 Experimental conditions

Spectra of NO_3 were obtained in flow cells heated to > 40ºC using the thermal decomposition of dinitrogen pentoxide (N_2O_5). The synthesis of N_2O_5 is described in Appendix 3.3. The pulsed CRDS apparatus was described in Chapter 2. The optical cavity consisted of a 50-cm long Pyrex cell wrapped in heating tape (T = 40-160ºC) with 13-cm purge volume couplers attached at each end to protect the CRD mirrors (LGR 1400 nm, R = 99.995%). Scans were collected at 0.2 and 0.4 cm^{-1} step size with helium/oxygen carrier gas (10-15 Torr) flowing through a N_2O_5 trap (T = -12ºC salt water/liquid nitrogen bath), with $P_{vapor,\ N2O5}$ ~ 1.5 Torr. The chemical identity of the bands was verified using N_2O_5 photolysis at 193 nm.

In our previous CRDS study, we flowed ozone at room temperature over the N_2O_5 trap to produce NO_3 radicals. In this study, we observed a > 5-fold increase in the NO_3 concentration under heated conditions (T = 40ºC). The residual water in the cell was also reduced, minimizing formation of nitric acid:

$$H_2O + N_2O_5 \rightarrow 2\ HNO_3 \qquad (3.4)$$

Nitric acid absorption in the NIR is discussed in Appendix 3.4. Absolute concentrations of NO_3 were measured via single-pass direct absorption with a diode laser (Sanyo diode DL 6147-040, 662 nm). Typical NO_3 concentrations were 10^{14} molec cm^{-3}.

3.4 Observed Spectra

3.4.1 Assignments

We observed several vibronic bands in the CRD spectrum of NO_3 in the 7000-7650 cm^{-1} region (Fig. 3.5). Assignments were aided by the distinct rotational contours of parallel and perpendicular bands of the $\tilde{A} \leftarrow \tilde{X}$ transition of NO_3. We modeled the contours using PGopher v. 5.3, developed by C. M. Western from the University of Bristol, to determine band origins of the observed bands (Appendix 3.5). The results have been summarized in Table 3.2, with schematics of the assigned bands shown in Figure 3.6.

Hot bands

Upon heating to 40°C, several absorption bands increased in intensity relative to the most intense band in the region, the 4_0^1 band at 7602.8(2) cm^{-1}. We definitively assigned three of these to hot bands of the $\tilde{A} \leftarrow \tilde{X}$ transition arising from thermal population of the lowest vibrational excited state 4_1: the 4_1^1 ($||$), $4_1^0 2_0^1$ ($\perp$), and $4_1^0 1_0^1$ ($||$) bands. Uncertainties in the band origins (1.0~3.0 cm^{-1}) were due to overlap of multiple hot bands. Other features that were observed but not assigned (* in Fig. 3.5), were attributed to hot bands of NO_3 based on their temperature dependence.

4_1^0 *hot band*

We collected CRD spectrum of the 4_1^0 hot band of NO_3 in the 6650-6710 cm^{-1} region. We compared the spectrum to a high resolution off-axis integrated cavity output spectrum (OA-ICOS) of the 4_1^0 band that had been previously obtained by our group and found the two spectra matched (Fig. 3.7).[51] A brief summary of the OA-ICOS experiment is

provided in Appendix 3.6. Analysis with an asymmetric top model led to assignment of the band origin to 6696.5(1.0) cm^{-1}. The band contour resembled the contours of the 4_0^n parallel bands, with a sharp R branch head and a gap near the origin.

Bandhead (cm^{-1})	**Intensity**	**Band origin (cm^{-1})**	**Assignment**
6703.906	w	6696.5(1.0)	4_1^0
7066.1, 7074.2	v. w.	7062.25(0.5)	0_0^0
7086.1	v. v. w.	-	
7243.1	w.	7235.5(1.5)	4_1^1
7375.8	w.	7370.0(3.0)	$4_1^0 2_0^1$
7434.7	v. w.	-	
7489.6	v. w.	7481.0(1.5)	$4_1^0 1_0^1$
7532.7	v. w.	-	
7610.6	s.	7602.8(2), **7602.5754(16)**	4_0^1
7745.5	s.	7740.9(3)*****, **7744**	2_0^1

Bold: Hirota and Kawaguchi high resolution studies
*****: observed in our previous CRD study
w = weak, v = very, s = strong

Table 3.2. Assignments of the observed $\tilde{A} \leftarrow \tilde{X}$ vibronic bands of NO_3

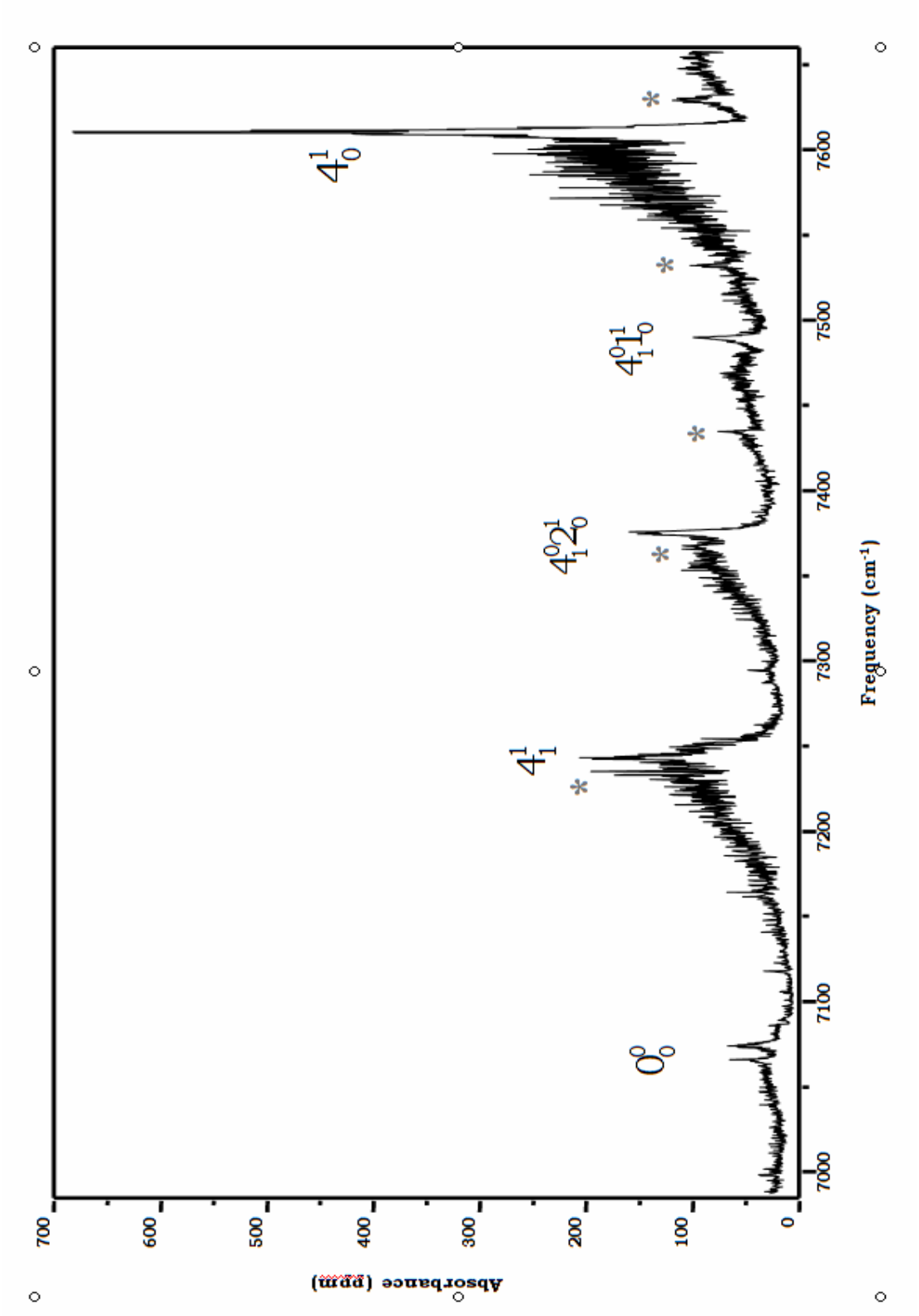

Figure 3.5. CRD spectrum of the $\tilde{A} \leftarrow \tilde{X}$ transitions of NO_3 in the 7000-7600 cm^{-1} NIR region. * = observed but unassigned hot bands of NO_3.

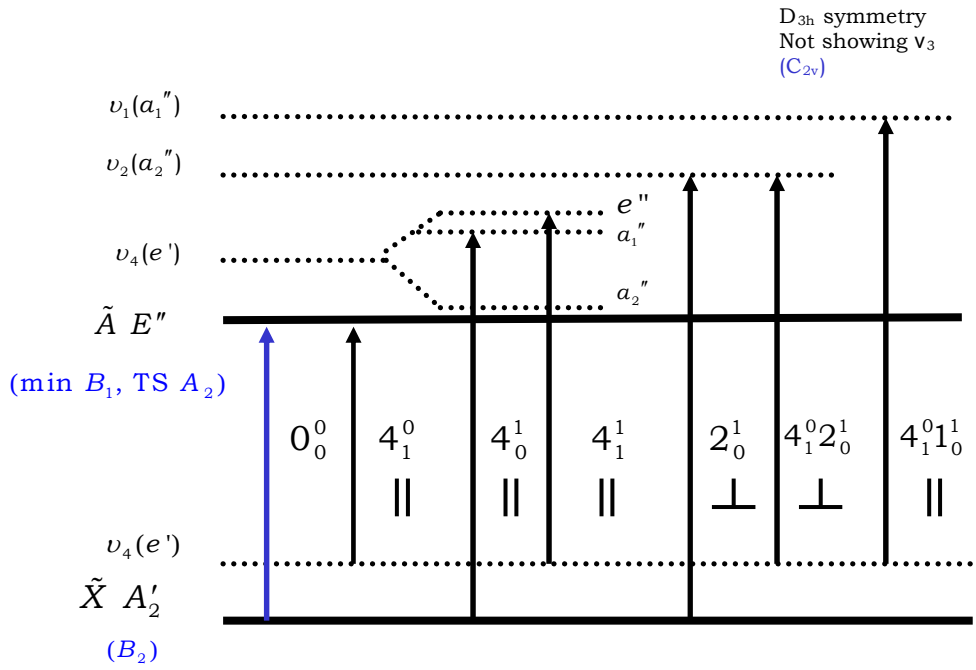

Figure 3.6. Diagram of the observed $\tilde{A} \leftarrow \tilde{X}$ vibronic bands of NO_3 in this work.

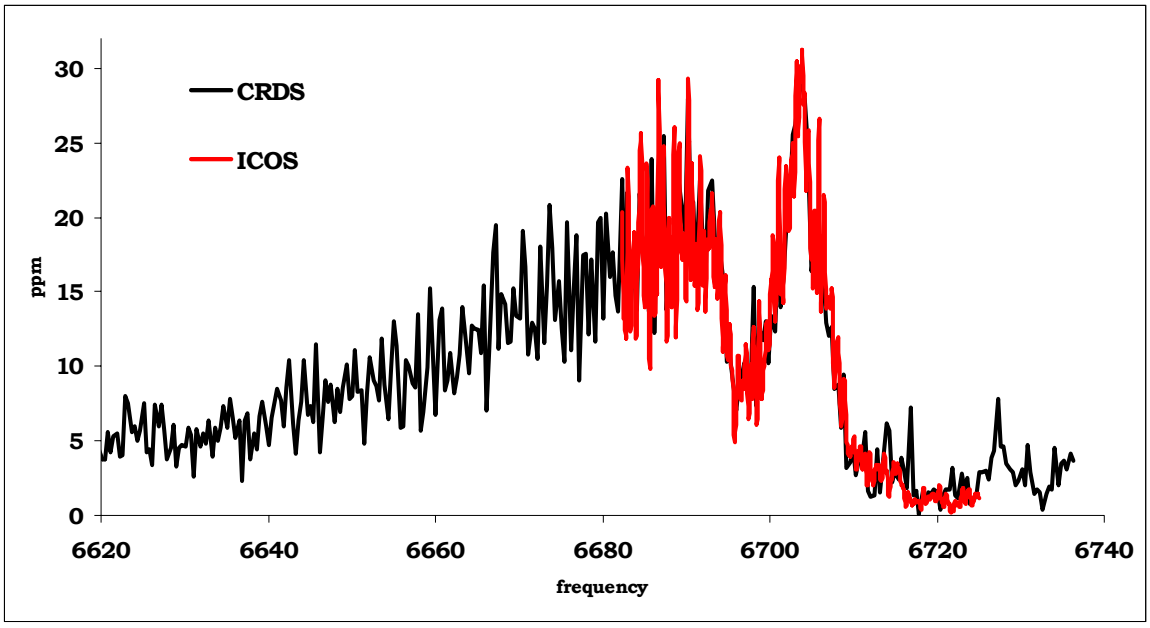

Figure 3.7. Comparison of the 4_1^0 hot band obtained by CRDS apparatus and the ICOS apparatus. The ICOS data was convoluted to a lower resolution (0.1 cm^{-1}) for comparison.

0_0^0 *origin band*

We observed a weak spectrum in the 7000-7100 cm^{-1}, in the vicinity of the expected origin (Fig. 3.8). The feature comprised of a broad underlying absorption from 7020-7080 cm^{-1} with two distinct Q-branch-like peaks at 7066.1 and 7074.2 cm^{-1} and a sharp edge at 7090 cm^{-1}. The rise in the absorption below 7020 cm^{-1} is due to the first overtone of the OH stretch of nitric acid impurities.

Variation of the intensity with temperature (T = 40-160 °C) indicated that the main features were not due to hot bands, with exception of the sharp edge, which grew with temperature. We therefore believe some of the features can be assigned to the magnetic dipole allowed origin band 0_0^0. We also scanned 700 cm^{-1} to the blue of the band to observe the $1_0^1 0_0^0$ band for confirmation; however the observed absorption was very weak and inconclusive (Fig. 3.9).

Contour analysis of the absorption at 7000-7100 cm^{-1} with magnetic dipole and electric quadrupole models could not fully reproduce all of the features, in particular the presence of two strong peaks. Simultaneous fits of the 0_0^0 magnetic transition and 4_1^0 vibronic transition bands led us to *tentatively* assign the first observed peak to the 0_0^0 transition with band origin at 7062.25(0.5) cm^{-1} and the second peak to an unidentified absorption by NO_3 or some contaminant with fortuitous absorption in the 7000-7100 cm^{-1} region. We discuss the second peak further in section 3.5. Given our assignment of the origin band, we used the measured NO_3 concentration to calculate the integrated cross section for the origin band to be 1.3×10^{-20} cm. We compared the integrated absorption cross sections of the 4_0^1 and 0_0^0 bands and found ratio = 25:1.

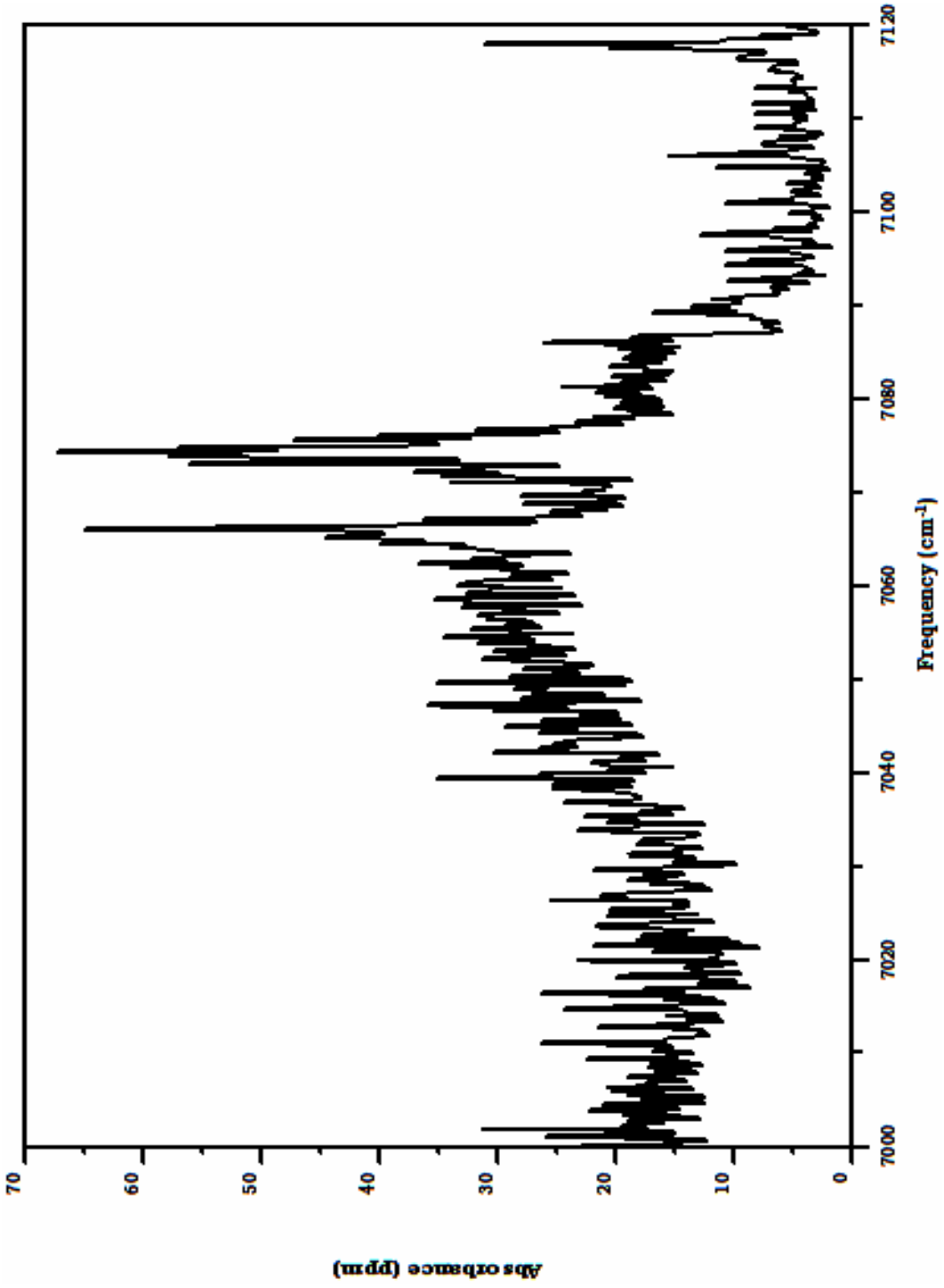

Figure 3.8. CRD spectrum of the origin of the $\tilde{A} \leftarrow \tilde{X}$ transition of NO_3.

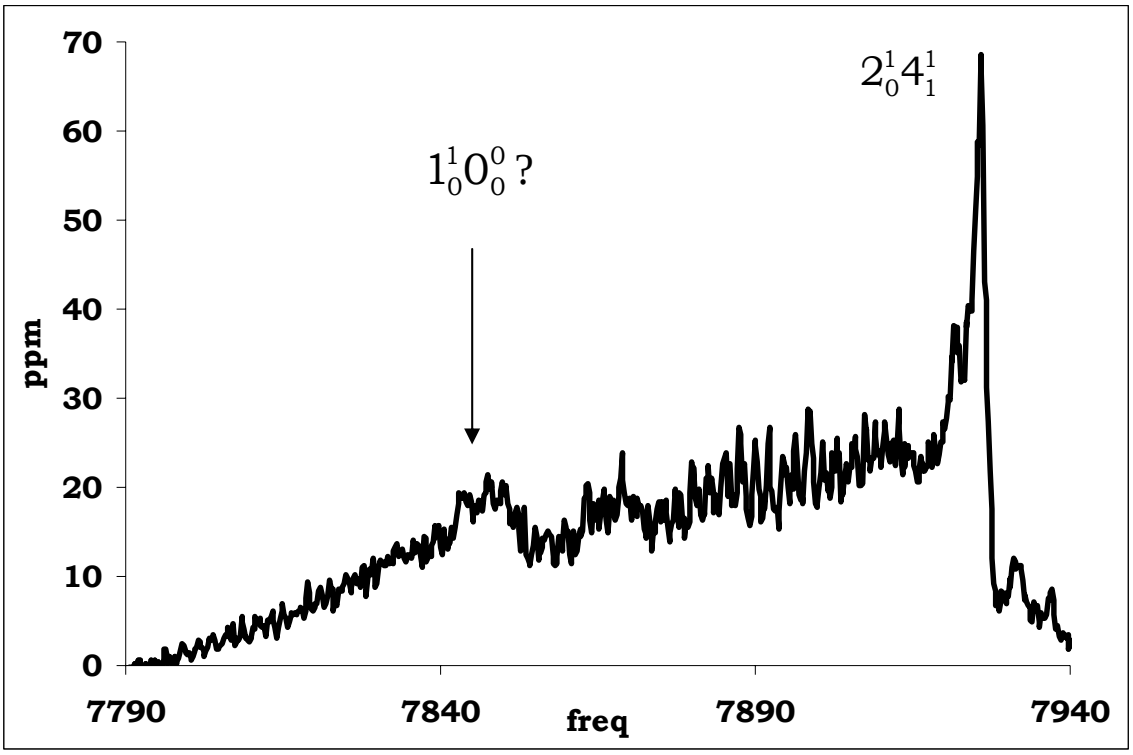

Figure 3.9. CRD spectrum of the 7790-7940 cm^{-1} region of NO_3. A weak absorption is observed near 7850 cm^{-1}, approximately 800 cm^{-1} (~υ_1) to the blue of the observed origin band of the $\tilde{A} \leftarrow \tilde{X}$ transition of NO_3.

$2_0^1 4_0^1$ *anomalous strong band*

In our previous CRDS study, we had tentatively assigned the anomalously strong band at 8287 cm^{-1} to the 3_0^1 band. We repeated the CRDS experiments at room and heated conditions (Fig. 3.10). We now reassign the band to $2_0^1 4_0^1$. The reassignment is discussed in detail in the discussion section.

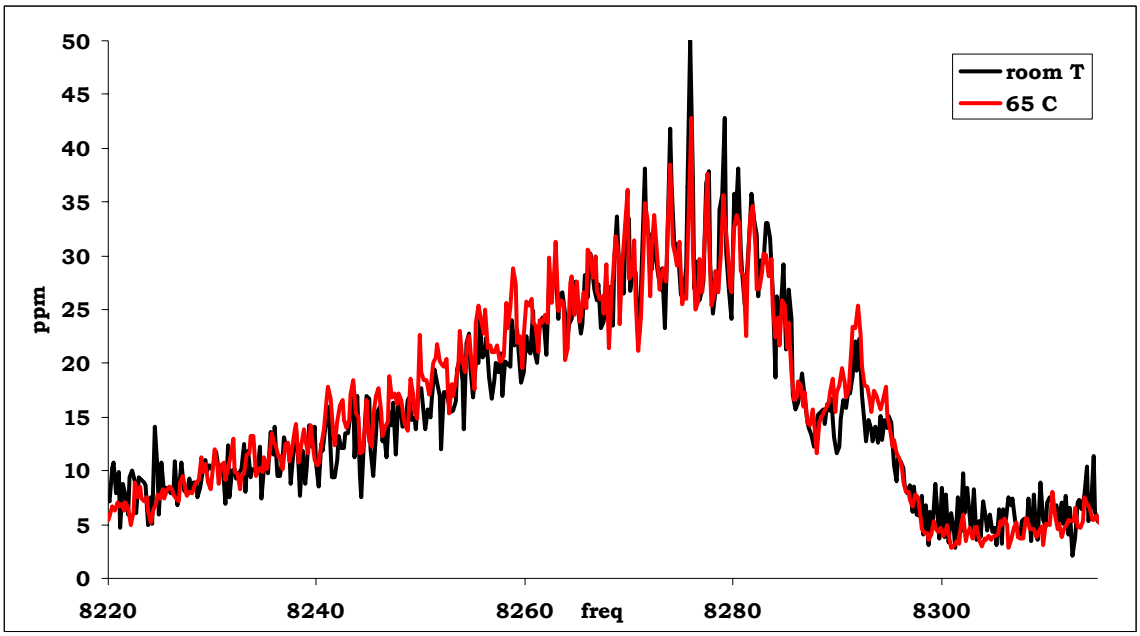

Figure 3.10. CRD spectra of NO_3 in the 8220-8350 cm^{-1} region at room and T = 65˚C temperatures. The anomalously strong absorption at 8287 cm^{-1} is reassigned to the $2_0^1 4_0^1$ band.

3.4.2 Fundamental vibrations

Many of the fundamental vibrations in both the ground and $\tilde{A}$ states of NO_3 can be calculated from the assigned bands. The frequencies of the fundamental vibrations are summarized in Table 3.3.

Ground state υ_4''

The ground state υ_4'' level has only been recently observed directly via absorption methods. Jacox *et al.* and Kawaguchi *et al.* reported υ_4'' = 365.6 cm^{-1} and υ_4'' = 365.48419 cm^{-1} in FTIR matrix and gas phase experiments, respectively.[36,52] Previous studies had involved LIF detection, with estimates of υ_4'' varying from 360-380 cm^{-1}. From

combination differences between $0_0^0 - 4_1^0$, we calculated υ_4'' = 365.75(1.1) cm^{-1}.

THE GROUND STATE VIBRATIONAL FREQUENCY

Vibrational level	Expt. Freq. (cm^{-1})	Method	Calc. Freq. (cm^{-1})	Method
υ_4 (e')	380	LIF [18]		
	360/418	LIF [19]	272.9	MR-SDCI [16]
	368	LIF [20]	246	EOMIP-CCSD [45]
	365	CRDS [24]	249	EOMIP-CCSD [45]
	365.6	Matrix FTIR [22]	361	LVC [13]
	365.48419	FTIR [52]		
	365.75(1.1)	**CRDS**		

THE Ã STATE VIBRATIONAL FREQUENCIES

Vibrational level	Expt. Freq. (cm^{-1})	Method	Calc. Freq.(cm^{-1})	Method
υ_1 (a_1')	804(4)	Anion PES [32]	820	CCSD(T) [45]
	785*	CRDS [24]	905	MR-SDCI [16]
	783.1/782.5*	Matrix FTIR [36]	801.8	EOMIP-CCSD [45]
	784.5(1.8)	**CRDS**		
υ_2 (a_2'')	683	IR Diode [34]	685	CCSD(T) [45]
	678	CRDS [24]	730.7	MR-SDCI [16]
	656/680.6	Matrix FTIR [36]	738	EOMIP-CCSD [45]
	678.65(58)	**CRDS**		
υ_3 (e')	1223?	CRDS [24]	1292/1569	CCSD(T) [45]
			1230/1595	MR-SDCI [16]
			1216.7/1754.8	EOMIP-CCSD [45]
υ_4 (e')	541(8)	Anion PES [32]	566/567	CCSD(T) [45]
	519-547*	CRDS [24]	373.7/270.9	MR-SDCI [16]
	514.2-558.3*	Matrix FTIR [36]	681/588	EOMIP-CCSD [45]
	540.55(54)	**CRDS**		

Bold: results from this work; * = assignment from combination band

Table 3.3. Comparison of the vibrational frequencies of NO_3 determined in this work with previous theoretical and experimental values.

Ã state υ_1'

Transitions to the υ_1' level from the ground state are forbidden by HT selection rules. We used the combination difference between the $4_1^0 1_0^1 - 4_1^0$ bands to calculate υ_1' = 784.5(1.8) cm^{-1}. Past absorption studies have relied on extricating the value of υ_1' from allowed transitions

$4_0^n 1_0^1$ and $2_0^1 1_0^1$. Combination differences between $4_0^n 1_0^1 - 4_0^{n-1}$ (n = 1, 2) bands were used by both Deev *et al.* and Jacox *et al.* to estimate υ_1' = 763-779 cm^{-1} and υ_1' = 733.7-763.2 cm^{-1} respectively, with the wide frequency range attributed to JT effects along the Q_4 coordinate.[24,36] The difference in the $2_0^1 1_0^1 - 2_0^1$ bands predicted a larger value for υ_1', υ_1' = 785 cm^{-1} and υ_1' = 782.5-783.1 cm^{-1}, respectively. The latter estimates are more reliable as they involved non-JT active modes and agree with our assessment.

$\tilde{A}$ state υ_2'

The fundamental frequency υ_2' was directly calculated from the 2_0^1 and origin bands. We found υ_2' = 678.65(68) cm^{-1}, which is well within the experimental limits of previous studies.

To check our other band assignments, we calculated υ_2' and υ_4'' from the combination differences between $4_1^0 2_0^1 - 4_1^0$ and $2_0^1 - 4_1^0 2_0^1$. We found υ_2' = 673.5(3.2) cm^{-1} and υ_4'' = 370.9(3.0) cm^{-1}, respectively. The $4_1^0 2_0^1$ hot band was difficult to simulate due to convolution of multiple hot bands. Interestingly, if the band origin for the $4_1^0 2_0^1$ band were shifted to the blue by 5 cm^{-1}, both calculated vibrational levels would be within errors of the frequency values calculated directly from the observed origin band 0_0^0.

$\tilde{A}$ state υ_3'

The υ_3' level was not observed in this study. More details can be found in the discussion section.

$\tilde{A}$ state $\upsilon_4' = a_1''$

As a degenerate mode, the $\tilde{A}^2E'' \otimes \upsilon_4(e')$ manifold is split into three vibronic levels: $a_1'' \oplus a_2'' \oplus e''$. HT selection rules only allow transitions to the a_1'' level from the ground state. Current literature values for υ_4' all refer to the a_1'' level. We thus calculated $\upsilon_4' = a_1''$ from $4_0^1 - 0_0^0$ to be 540.55(54) cm^{-1}. This is consistent with previous measurements.

3.4.3 Jahn Teller splitting in the $\upsilon_4' = 1$, E'' × e' level

We used the 4_1^1 band to probe the e'' level of the $\tilde{A}^2E'' \otimes \upsilon_4(e')$ manifold. Along with other measurements, we calculated the JT splitting *JT(a_1'' - e'')* from the relation $(4_1^1 + \upsilon_4'') - 4_0^1$ to be -1.55(1.9) cm^{-1}. The relatively small magnitude of the splitting is consistent with previous observations of small to moderate JT coupling strength in the Q_4 coordinate.

3.5 Discussion

We observed the origin of the $\tilde{A} \leftarrow \tilde{X}$ transition of NO_3 for the first time in the gas phase. The band origin was assigned to $T_0(\tilde{A})$ = 7062.25(0.5) cm^{-1}, with integrated absorption cross section for the band ~1.3 × 10^{-20} cm. From the assignment, we determined all the fundamental vibrational levels of the Ã state except υ_3'. We also identified several 4_1^X hot bands in the 7000-7650 cm^{-1} region. From the 4_1^1 band, we calculated the splitting in the $\tilde{A}^2E'' \otimes \upsilon_4(e')$ manifold, *JT(a_1'' - e'')* = -1.55(1.9) cm^{-1}. This was the first quantitative measurement of the JT activity along the Q_4 mode.

A comparison of our experimental vibrational frequencies to the calculated values was shown in Table 3.3. As MRCI calculations predict a large JT distortion for the $\tilde{A}$ state, vibrational frequencies were calculated for the $\tilde{A}$ state (B_1) assuming C_{2v} symmetry. Table 3.3 shows that adiabatic models cannot quantitatively describe the $\tilde{A}$ state accurately, although CCSD(T) does surprisingly well. Non-adiabatic effects therefore must be included to model NO_3 correctly. Several groups have begun to use the LVC model to include PJT effects. The LVC model has already been used to calculate ground state vibrational frequencies of NO_3 with great quantitative success.[13] No one however has used the LVC model to directly study the origin band of the $\tilde{A} \leftarrow \tilde{X}$ transition of NO_3. In fact, no theoretical work has been done on the magnetic dipole transitions of NO_3.

The LVC model has been used by Faraji *et al.* to predict a small JT distortion along the Q_4 coordinate and a very strong JT distortion along the Q_3 coordinate for NO_3.[43] This could explain the difficulties in observing the 3_0^1 band, as poor Franck-Condon overlap should lead to very weak absorption. In our previous CRD study, we had tentatively assigned the anomalously strong absorption at 8287 cm^{-1} to the 3_0^1 band (Fig. 3.10). The difference between the 3_0^1 and 0_0^0 band is approximately $\upsilon_2' \oplus \upsilon_4'$. If the anomalous band is reassigned to the $2_0^1 4_0^1$ band, the anomalous strong absorption could be explained by intensity borrowing from the "zero-frequency" electronic transition between the $\tilde{A}^2E''$ state components via strong quadratic PJT coupling between the $\tilde{A}$ and $\tilde{X}$ states (Fig. 3.11). The dipole moment between the $\tilde{A}^2E''$ state components is estimated to be quite strong (~1.2 Debeye).[53] Weak absorptions observed in the 8760 cm^{-1} region in the previous CRD study

would then be the best candidates for the 3_0^1 band (υ_3'~1697 cm^{-1}). The high density of bands in the region however makes definitive assignment difficult. Improved theoretical calculations of the vibrational frequencies in the Ã state would help us definitively assign the 3_0^1 band.

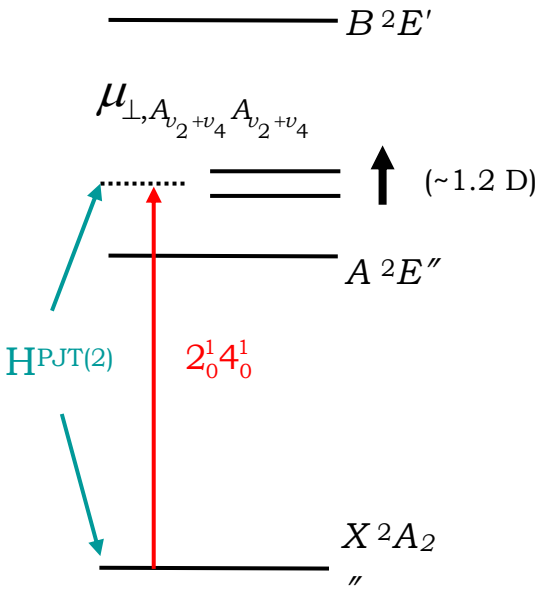

Figure 3.11. Schematic of intensity borrowing mechanism for the anomalous $2_0^1 4_0^1$ band. The "zero-frequency" transition can be compared to the first order Starks effect.

While we have provided many new benchmarks for *ab initio* models, open experimental questions on the *Ã* state remain. The most obvious issue is the resolution of the two observed peaks in the origin region. Our assignment of the first peak to the origin band is consistent with other groups' estimates of the origin band: $T_0(\tilde{A})$ = 7000(110) cm^{-1}, 7061(8) cm^{-1}, 7064 cm^{-1}, and 7058.5 cm^{-1}, respectively.[24,32,33,36] The second peak is located only 8 cm^{-1} to the blue of the first peak. As the second peak also grows relative to the concentration of NO_3, the peak appears to belong to NO_3. From our temperature experiments, we rule out the possibility that the second peak is a hot band. The feature is also too strong to be an electric quadrupole transition.

The second peak has a rotational contour similar to the parallel 4_0^1 band. Of the $\tilde{A}^2E'' \otimes \upsilon_4(e') = a_1'' \oplus a_2'' \oplus e''$ manifold, the a_1'' and e'' levels have been observed via the 4_0^1 and 4_1^1 bands, respectively. Only the a_2'' level has never been observed. Its energy level has been predicted to be ~10 cm^{-1} above the zero point of the $\tilde{A}$ state.[53] This corresponds roughly to the observed shift in the second peak from the origin band.

Transitions from the ground state to the a_2'' level however are forbidden. This can be shown by examination of the symmetry of the total wavefunction Ψ_{tot} for NO_3:

$$\Psi_{tot} = \Gamma_{elec} \times \Gamma_{vibr} \times \Gamma_{rot} \times \Gamma_{nuclr} \tag{3.5}$$

Assuming D_{3h} symmetry (or subgroup D_3), Ψ_{tot} should remain the same upon exchange of the oxygen atoms (bosons, with $I = 0$):

$$\hat{P}_{12}\Psi_{tot} = +\Psi_{tot}. \tag{3.6}$$

Then,

$$\begin{aligned} &A_1 \in \Psi_{tot} = \Gamma_{elec} \times \Gamma_{vibr} \times \Gamma_{rot} \times \Gamma_{nuclr} \\ &= \Gamma_{elec} \times \Gamma_{vibr} \times \Gamma_{rot} \otimes A_1 \Rightarrow \Gamma_{elec} \times \Gamma_{vibr} \times \Gamma_{rot} = A_1 \end{aligned}. \tag{3.7}$$

Assuming $\Gamma_{elec} = A_1$ and $\Gamma_{vibr} = A_1$, for $K = 0$, even J levels have A_1 symmetry, while odd J levels have A_2 symmetry. For $K = 3n$, the J levels have both A_1 and A_2 symmetry, while for $K \neq 3n$, the J levels have E symmetry.[54]

The ground state of NO_3 has A_2 symmetry ($\Gamma_{elec} \otimes \Gamma_{vibr} = A_2$). Thus, from equation (3.7), only odd J'' levels of $K'' = 0$ and J'' levels of $K'' = 3n$ are allowed. The selection rules for a parallel band state that: $\Delta K = 0$, with $\Delta J = \pm 1$ for $K'' = 0$ and $\Delta J = 0, \pm 1$ for $K'' \neq 0$. Then for $K' = 0$, only even J'' levels (A_1) are allowed. In the $\tilde{A}^2E'' \otimes \upsilon_4(e')$ manifold, equation (3.7) implies that only the vibronic state with A_1 symmetry is allowed. A new mechanism is therefore needed to explain observation of the a_2'' level.

One possible mechanism is the inclusion of rotationally forbidden states. Oka *et al.* used this mechanism to explain the observation of the forbidden $\upsilon_1 \leftarrow 0$ ($A_1 \leftarrow A_1$) transition in H_3^+.[55] More explicitly, the rovibrational transition υ_1, J', $K'+3 \leftarrow J''$, K'' borrows intensity from the allowed $\upsilon_2 \leftarrow 0$ ($A_2 \leftarrow A_1$) or υ_2, $l = 1$, J', $K'+1 \leftarrow J''$, K'' transition in H_3^+. To better understand the mechanism, consider a simple basis set for a molecule, consisting of the product of vibrational and rotational wavefunctions:

$$\Gamma_{vibr} \otimes \Gamma_{rot} \Rightarrow \; |\upsilon\rangle |J \; K\rangle . \qquad (3.8\text{ a})$$

The wavefunction of a specific energy level is described by the linear combination of the basis set (3.8 a). The symmetry of the individual components must retain the same symmetry as the overall wavefunction. Under this analysis, the υ_1 and υ_2 states of H_3^+ cannot interact:

$$|\upsilon_1\rangle + \lambda |\upsilon_2\rangle \Rightarrow A_1 + A_2 . \qquad (3.9\text{ a})$$

If the vibronic basis set

$$\Gamma_{vibr} \otimes \Gamma_{rot} \Rightarrow \quad |\upsilon \;\; J \;\; K\rangle \tag{3.8 b}$$

is used, then the symmetries of the rotational levels can differ for each respective state to allow coupling:

$$|\upsilon_1 \;\; J \;\; K_1\rangle + \lambda\, |\upsilon_2 \;\; J \;\; K_2\rangle \Rightarrow (A_1 \otimes A_2) + (A_2 \otimes A_1) = A_2 + A_2 \tag{3.9 b}$$

Thus, the forbidden $\upsilon_1 \leftarrow 0$ transition borrows intensity from the allowed $\upsilon_2 \leftarrow 0$ transition. A similar mechanism may be leading to the observation of the second peak in the NO_3 spectrum. More experimental and especially theoretical investigations however are needed.

This CRD study represents the only experimental work that has examined the $\tilde{A} \leftarrow \tilde{X}$ hot bands of NO_3. While we have focused primarily on the $\tilde{A}$ state, the hot bands can also shed light on the ground state of NO_3. We have already demonstrated this by determining the υ_4'' level from the observed hot bands. There is current disagreement in the literature over the value of υ_3'' (1492 cm^{-1} vs. 1000 cm^{-1}). If we take the latter assignment for υ_3'', many of the hot bands originating from the υ_3'' state would lie in the * regions of Figure 3.5. There are however, many other possible combination bands that could have absorptions in the same region. More experiments are clearly needed.

3.6 Summary

This chapter highlighted the quantitative advances we have made in elucidating the non-adiabatic effects of the $\tilde{A}$ state of NO_3. We observed the $\tilde{A} \leftarrow \tilde{X}$ magnetic-dipole allowed origin transition, along with several vibronic hot bands, using the pulsed CRDS apparatus. From analysis, we assigned the fundamental vibrational levels of the $\tilde{A}$ state of NO_3 and calculated the JT splitting in the $\tilde{A}^2E'' \otimes \upsilon_4(e')$ manifold. As a small radical system with both JT and PJT effects, NO_3 is a benchmark system for many non-adiabatic models. Our work helped define areas in which theoretical models still need to be developed. Further experimental and theoretical collaborations are planned.

Now that we better understand the chemical physics of NO_3, we are ready to examine the role of NO_3 in our atmosphere. We are specifically interested in the oxidation of various volatile organic compounds by NO_3 at nighttime. We discuss these issues in the following chapter.

3.7 References

(1) Finlayson-Pitts, B. J.; Pitts, J. N. *Chemistry of the Upper and Lower Atmosphere: Theory, Experiments, and Applications*; Academic Press: San Diego, CA, 2000.

(2) Seinfeld, J. H.; Pandis, S. N. *Atmospheric Chemistry and Physics*; Wiley-Interscience, 1997.

(3) Wayne, R. P.; Barnes, I.; Biggs, P.; Burrows, J. P.; Canosamas, C. E.; Hjorth, J.; Lebras, G.; Moortgat, G. K.; Perner, D.; Poulet, G.; Restelli, G.; Sidebottom, H. *Atmospheric Environment Part a - General Topics* **1991**, *25*, 1.

(4) Chappuis, J. *Ann. d. l" ecole Norm. Sup.* **1882**, *11*, 159.

(5) Walsh, A. D. *Journal of the Chemical Society* **1953**, 2301.

(6) Jahn, H. A.; Teller, E. *Proc. R. Soc. Lond. A - Math. Phys. Sci.* **1937**, *161*, 220.

(7) Longuethiggins, H. C.; Opik, U.; Pryce, M. H. L.; Sack, R. A. *Proc. R. Soc. Lond. A - Math. Phys. Sci.* **1958**, *244*, 1.

(8) Opik, U.; Pryce, M. H. L. *Proc. R. Soc. Lond. A - Math. Phys. Sci.* **1957**, *238*, 425.

(9) Applegate, B. E.; Barckholtz, T. A.; Miller, T. A. *Chemical Society Reviews* **2003**, *32*, 38.

(10) Barckholtz, T. A.; Miller, T. A. *International Reviews in Physical Chemistry* **1998**, *17*, 435.

(11) Kaldor, U. *Chemical Physics Letters* **1991**, *185*, 131.

(12) Eisfeld, W.; Morokuma, K. *Journal of Chemical Physics* **2000**, *113*, 5587.

(13) Stanton, J. F. *Journal of Chemical Physics* **2007**, *126*.

(14) Davy, R. D.; Schaefer, H. F. *Journal of Chemical Physics* **1989**, *91*, 4410.

(15) Crawford, T. D.; Stanton, J. F. *Journal of Chemical Physics* **2000**, *112*, 7873.

(16) Eisfeld, W.; Morokuma, K. *Journal of Chemical Physics* **2001**, *114*, 9430.

(17) Wladyslawski, M.; Nooijen, M.; Hoffmann, M. R., Dyall, K. G., Eds. 2002, p 65.

(18) Ishiwata, T.; Fujiwara, I.; Naruge, Y.; Obi, K.; Tanaka, I. *Journal of Physical Chemistry* **1983**, *87*, 1349.

(19) Nelson, H. H.; Pasternack, L.; McDonald, J. R. *Journal of Physical Chemistry* **1983**, *87*, 1286.

(20) Kim, B. S.; Hunter, P. L.; Johnston, H. S. *Journal of Chemical Physics* **1992**, *96*, 4057.

(21) Friedl, R. R.; Sander, S. P. *Journal of Physical Chemistry* **1987**, *91*, 2721.

(22) Jacox, M. E.; Thompson, W. E. *Journal of Chemical Physics* **2008**, *129*.
(23) Kawaguchi, K.; Hirota, E.; Ishiwata, T.; Tanaka, I. *Journal of Chemical Physics* **1990**, *93*, 951.
(24) Deev, A.; Sommar, J.; Okumura, M. *Journal of Chemical Physics* **2005**, *122*.
(25) Jones, E. J.; Wulf, O. R. *Journal of Chemical Physics* **1937**, *5*, 873.
(26) Matsumoto, J.; Imai, H.; Kosugi, N.; Kaji, Y. *Atmospheric Environment* **2005**, *39*, 6802.
(27) Matsumoto, J.; Imai, H.; Kosugi, N.; Kajii, Y. *Chemistry Letters* **2005**, *34*, 1214.
(28) Matsumoto, J.; Kosugi, N.; Imai, H.; Kajii, Y. *Review of Scientific Instruments* **2005**, *76*.
(29) Brown, S. S.; Osthoff, H. D.; Stark, H.; Dube, W. P.; Ryerson, T. B.; Warneke, C.; de Gouw, J. A.; Wollny, A. G.; Parrish, D. D.; Fehsenfeld, F. C.; Ravishankara, A. R. *Journal of Photochemistry and Photobiology a - Chemistry* **2005**, *176*, 270.
(30) Wood, E. C.; Wooldridge, P. J.; Freese, J. H.; Albrecht, T.; Cohen, R. C. *Environmental Science & Technology* **2003**, *37*, 5732.
(31) Carter, R. T.; Schmidt, K. F.; Bitto, H.; Huber, J. R. *Chemical Physics Letters* **1996**, *257*, 297.
(32) Weaver, A.; Arnold, D. W.; Bradforth, S. E.; Neumark, D. M. *Journal of Chemical Physics* **1991**, *94*, 1740.
(33) Hirota, E.; Ishiwata, T.; Kawaguchi, K.; Fujitake, M.; Ohashi, N.; Tanaka, I. *Journal of Chemical Physics* **1997**, *107*, 2829.
(34) Kawaguchi, K.; Ishiwata, T.; Hirota, E.; Tanaka, I. *Chemical Physics* **1998**, *231*, 193.
(35) Deev, A., *Ph. D. Thesis*, California Institute of Technology, 2004.
(36) Jacox, M. E.; Thompson, W. E. *Journal of Physical Chemistry A* **2009**.
(37) Liu, J. J.; Chen, M. W.; Melnik, D.; Yi, J. T.; Miller, T. A. *Journal of Chemical Physics* **2009**, *130*.
(38) Endo, Y.; Saito, S.; Hirota, E. *Journal of Chemical Physics* **1984**, *81*, 122.
(39) Momose, T.; Endo, Y.; Hirota, E.; Shida, T. *Journal of Chemical Physics* **1988**, *88*, 5338.
(40) Viel, A.; Eisfeld, W. *Journal of Chemical Physics* **2004**, *120*, 4603.
(41) Mahapatra, S.; Eisfeld, W.; Koppel, H. *Chemical Physics Letters* **2007**, *441*, 7.

(42) Koppel, H.; Domcke, W.; Cederbaum, L. S. *Advances in Chemical Physics* **1984**, *57*, 59.
(43) Faraji, S.; Koppel, H.; Eisfeld, W.; Mahapatra, S. *Chemical Physics* **2008**, *347*, 110.
(44) Stanton, J. F.; Okumura, M. *Physical Chemistry Chemical Physics* **2009**, *11*, 4742.
(45) Okumura, M.; Stanton, J. F.; Deev, A.; Sommar, J. 2006, p C64.
(46) Bernath, P. *Spectra of Atoms and Molecules*; 2nd ed.; Oxford University Press: New York, 2005.
(47) Callomon, J. H.; Innes, K. K. *Journal of Molecular Spectroscopy* **1963**, *10*, 166.
(48) Lombardi, J. R.; Freeman, D. E.; Klempere.W *Journal of Chemical Physics* **1967**, *46*, 2746.
(49) Van Vleck, J. H. *Astrophysical Journal* **1934**, *80*, 161.
(50) Havey, D. K.; Long, D. A.; Okumura, M.; Miller, C. E.; Hodges, J. T. *Chemical Physics Letters* **2009**, *483*, 49.
(51) Robichaud, D. J., *Ph. D. Thesis*, California Institute of Technology, 2008.
(52) Kawaguchi, K.; Shimizu, N.; Fujimori, R.; Tang, J.; Ishiwata, T.; Tanaka, I. *J. Molecular Spectroscopy* **2011 (submitted)**.
(53) Stanton, J. F., Private communication.
(54) Herzberg, G. *Molecular Spectra and Molecular Structure (3 volume set)*; Kriger Pub., 1992.
(55) Xu, L. W.; Rosslein, M.; Gabrys, C. M.; Oka, T. *Journal of Molecular Spectroscopy* **1992**, *153*, 726.